

Full Length Article

Atomic interface structure and electronic properties at nanoscale rotated crystal in Ga_2O_3 homoepitaxial film

Trong Si Ngo^{a,1}, Soon-Ku Hong^{a,*}, Hyeon Woo Kim^{b,1}, Sung Beom Cho^{b,*}, Young Heon Kim^{c,*}, Nguyen Quoc Vuong^a, Hu Young Jeong^d, Raouf Hayyak^a, Taswar Iqbal^a, Dae-Woo Jeon^e, Ji-Hyeon Park^e, Jae Kyoung Mun^f

^a Department of Materials Science and Engineering, Chungnam National University, Daejeon 34134, Republic of Korea

^b Department of Materials Science and Engineering, Ajou University, Suwon 16499, Republic of Korea

^c Graduate School of Analytical Science and Technology (GRAST), Chungnam National University, Daejeon 34134, Republic of Korea

^d Graduate School of Semiconductor Materials and Devices Engineering, Ulsan National Institute of Science and Technology (UNIST), Ulsan 44919, Republic of Korea

^e Display Materials Center, Korea Institute of Ceramic Engineering and Technology (KICET), Jinju, Gyeongsangnam-do 52851, Republic of Korea

^f Quantum Sensing Research Section, Electronics and Telecommunications Research Institute (ETRI), Daejeon 34129, Republic of Korea

ARTICLE INFO

ABSTRACT

Keywords:
Gallium oxide
Epitaxy
Microscopy
Density functional theory
Interface structure
Electronic property

Although $\beta\text{-Ga}_2\text{O}_3$ is emerging as a next-generation power-electronics material, the understanding of two-dimensional defects is still lacking due to its complex crystal structure. We report a nanoscale rotated crystal of the $\beta\text{-Ga}_2\text{O}_3$ homoepitaxial layer and identify its crystal structure and electronic properties. By coordinating scanning transmission electron microscopy and density functional theory calculations, we analyze the rotated crystal in the homoepitaxial film with a crystallographic orientation of $(\bar{2}01)_{\text{rotated}}//(\bar{2}02)_{\text{matrix}}$ and $[010]_{\text{rotated}}//[010]_{\text{matrix}}$. The mismatch at the $(\bar{2}01)//(\bar{2}02)$ interface was as small as 0.0013, which is very close to zero. Subnanometer scale displacement of specific Ga atoms by $\sim 1.03 \text{ \AA}$, appearing repeatedly and regularly at the interface was found. From DFT calculation the interface formation energy was determined to be 75.3 mJ/m^2 , which is very small compared to stacking fault energy of semiconductor materials. In addition, this defect itself induces delocalized deep-level states and we further calculated changes in band structure by impurity segregation at the boundary, which are difficult to passivate with segregation of impurities. These results provide a fundamental understanding into the atomic-scale interfacial structure at the locally formed nanoscale defect and their electronic property.

1. Introduction

Homoepitaxy is the process of growing crystalline thin films of functional materials with different doping levels guided by substrates of the same material with well-defined orientations, which is used in a wide variety of fields, so its technological development to achieve high-quality growth is an inevitable issue for successful applications [1,2]. The fabrication of a perfect single-crystal in homoepitaxy is advantageous for achieving superior material properties, but it is challenging because of uncontrollable and unpredictable behaviours, such as pre-reactions of raw materials [3], distortions due to applied stresses [4], and misalignment of adatoms [5]. Because these factors can lead to the formation of intrinsic defects, including tilted atomic structures,

twinned interface boundaries, and point defects, understanding the fundamental mechanisms and their effect on the final properties of the materials is critical [6–10]. For example, in the case of high-power electronics based on wide-bandgap semiconductor materials, the materials must be defect-free because premature breakdown can occur due to the presence of local obstacles. Even atomic-scale defects have the potential to degrade electrical properties [11]. In addition, the structural complexity due to the high density of functional materials makes it difficult to achieve thin films with high crystallinity. This implies that analysing and defining atomic-scale defects is essential for the growth of close-to-ideal homoepitaxial layer.

Among the various functional semiconductor materials, Ga_2O_3 is emerging as a promising candidate for next-generation power

* Corresponding authors at: Department of Materials Science and Engineering, Chungnam National University, Daejeon 34134, Republic of Korea.

E-mail addresses: soonku@cnu.ac.kr (S.-K. Hong), csb@ajou.ac.kr (S.B. Cho), y.h.kim@cnu.ac.kr (Y.H. Kim).

¹ Trong Si Ngo and Hyeon Woo Kim contributed equally.

electronics because of its ultra-wide bandgap energy (4.8 eV) and a high predicted electrical breakdown field of 8 MV/cm, which exceeds the properties of GaN and SiC [12,13]. The monoclinic structure of Ga_2O_3 has received the most attention owing to its stable form under ambient conditions and commercially available substrates produced by cost-effective melt-based single-crystal-growth technology. Reported Ga_2O_3 -based power electronics demonstrated remarkable performance in devices such as Schottky barrier diode (SBD) [14–19] and field effect transistor (FET) [20–25]; however, a limitation is the formation of unintentional atomic defects in epitaxial films, which can weaken the performance of the application. This is primarily due to the complexity of the monoclinic structure and the diverse polymorphic nature of Ga_2O_3 [26]. While there have been numerous attempts to understand the atomic-scale defects for the fabrication of perfect single-crystal thin films [27], defining these defects is still a challenge because of the presence of various substrates with specific cleavage characteristics [28]. Therefore, an improved understanding of structural imperfections in homoepitaxially grown Ga_2O_3 thin films via systematic studies is critical to overcome technological challenges and promote their industrial application in power-electronic devices.

Recent studies on crystal defects in β - Ga_2O_3 have primarily focused on defects in β - Ga_2O_3 substrates [29–37]. In which, dislocations and their Burgers vectors have been extensively determined by synchrotron X-ray topography [29–35]. Void defects have been observed and reported the origin of reverse leakage current in the Schottky barrier diodes made with edge-defined film-fed grown (001) β - Ga_2O_3 substrate [30]. Bent-shaped twin boundary in β - Ga_2O_3 (010) and (100) substrates has been studied at atomic-scale through a combination of selective etching, transmission electron microscopy (TEM), and scanning transmission electron microscopy (STEM) [36]. First-principles calculations have also been performed to evaluate the energetics and electronic structure of twin boundaries and stacking faults in β - Ga_2O_3 [37]. In contrast to these investigations of the defects in β - Ga_2O_3 substrates, only a limited number of studies have explored extended defects in β - Ga_2O_3 films [5,38–42]. Furthermore, studies on defects in the β - Ga_2O_3 epilayer have almost focused on dislocations observed by synchrotron X-ray topography [38], STEM under polycrystalline defects [39], and stacking faults through selective etching, TEM, and STEM [40,41]. Only a few studies have reported rotated crystal defects such as twin and rotational domain in the β - Ga_2O_3 epitaxial layers [5,42].

By performing the defect selective etching and TEM observations, we have previously identified twin boundary defects in homoepitaxial β - Ga_2O_3 epitaxial layers grown on (201) β - Ga_2O_3 substrates by plasma-assisted molecular-beam epitaxy (PAMBE) [5]. Meng et al. observed the formation of rotational crystal β - Ga_2O_3 layers grown on (001) β - Ga_2O_3 substrates by MOCVD using X-ray diffraction and STEM [42]. However, there has been no investigation on the atomic-scale detailed interfacial structure and no theoretical study on the interface energy. Furthermore, there have been no reports on the effects of the extrinsic interfaces on the electronic properties of homoepitaxial β - Ga_2O_3 layers.

In this study, we report nanoscale rotated crystal defects in homoepitaxial β - Ga_2O_3 layers by coordinating atomic-scale microscopy and density functional theory (DFT) calculations. Using aberration-corrected high-angle annular dark-field (HAADF) STEM, the rotated crystal showed the (201)/(202) interface, which can be matched without any dangling bonds, even though the β - Ga_2O_3 has a low-symmetry monoclinic structure. This leads to the formation of interfacial boundaries and crystal defects that introduce misoriented growth of the rotated crystal from the original growth direction. The mismatch at the (201)/(202) interface was as small as 0.00136, which is 100 times smaller than that of (0001) GaN/sapphire interface. By DFT calculations we determined the interface energy of 75.3 mJ/m², which is very small as the order of stacking fault energy of GaN. We identified that this boundary locally creates a significant deep trap near the conduction bands, which significantly degrades its properties. Furthermore, even the segregation

of Si, H, or Al cannot easily prevent this type of defect.

Our findings in this study can provide insight to rotational crystal formation in monoclinic β - Ga_2O_3 homoepitaxial growth and material system, which has several different Miller indices planes but with the same d-spacings. Furthermore, our findings can provide fundamental understanding on the Ga_2O_3 and will be valuable in studies on its impact to properties of Ga_2O_3 -based electronic devices and development in the near future.

2. Experimental section

2.1. Epitaxial growth

The substrates were commercial Sn-doped (001) β - Ga_2O_3 epi-ready substrates synthesized by the edge-defined film-fed growth (EFG) method, with a thickness of 650 μm . The substrates were doped with Sn to a donor concentration of $7.3 \times 10^{18} \text{ cm}^{-3}$. The full width at half maximum (FWHM) values of omega rocking measurement using the X-ray diffraction method were 23 arcsec for the [100] azimuth and 25 arcsec for the [010] azimuth. The substrates were cleaned sequentially in methanol, acetone, and deionized (DI) water for 3 min using the ultrasonic agitation method. Later, the substrates were chemically cleaned in a solution of DI water: 30 % H_2O_2 ; 96 % H_2SO_4 = 1: 1 (vol.) for 5 min. They were then placed in DI flowing water for 15 min and dried under nitrogen flow. After chemical cleaning, the substrates were thermally cleaned in an oxygen plasma environment in a plasma-assisted molecular-beam epitaxy (PAMBE) growth chamber at 850 °C for 60 min. Homoepitaxial β - Ga_2O_3 layers were grown on (001) β - Ga_2O_3 substrates using PAMBE at a growth temperature of 850 °C. The base pressure in the growth chamber was of the order of $2.7 \times 10^{-7} \text{ Pa}$. The growth chamber was equipped with a reflection high-energy electron diffraction (RHEED) system for evaluating growth evolution. A standard effusion cell containing elemental gallium (Ga) with 6 N purity was used to supply the Ga flux, and a radio-frequency (RF) oxygen plasma source for supplying oxygen radicals was used. During the epitaxial growth, the RF plasma power and oxygen flow rate were set to 300 W and 2 sccm, respectively, and the Ga flux was set to 6 Å/min. The thickness of the Ga_2O_3 layer was approximately 150 nm.

2.2. Etch pit formation

To define the defect position for the low-defect-density and high-quality homoepitaxial β - Ga_2O_3 epilayer, the grown samples were etched in 85 % H_3PO_4 solution at 140 °C for various etching durations. Then, they were rinsed in DI water and dried using pure N_2 flow. The etched surfaces were observed using Nomarski optical microscopy (NOM) and scanning electron microscopy (SEM).

2.3. TEM specimen preparation

Cross-sectional specimens for scanning TEM (STEM) analysis were fabricated using a conventional Ga^+ ion-based focused ion beam (FIB) technique (Helios Nano Lab 450, FEI). In order to minimize potential Ga^+ ion beam-induced influence, further final thinning of the TEM specimen was performed with a low-energy Ar^+ ion milling system (Fischione Model 1040 Nanomill) operating with a state-of-the-art low energy of 50–2000 V. We applied 500 V for the final thinning. We believe the combining TEM specimen preparations by using Ga^+ ion-based FIB and a low-energy Ar^+ ion milling could effectively remove the energetic Ga^+ ion damaged layer on the surface of TEM specimen.

2.4. TEM and STEM characterizations

The TEM images were obtained using a JEOL JEM-ARM200F atomic resolution microscope with an accelerating voltage of 200 kV. HAADF HR-STEM images were obtained using a double Cs-corrected FEI Titan3

G2 60–300 microscope with an accelerating voltage of 200 kV.

2.5. Density functional theory calculations

To investigate the atomic and electronic structure of the abnormal $\beta\text{-Ga}_2\text{O}_3$ homoepitaxial layer, we performed first-principles DFT calculations using the Vienna ab initio simulation package (VASP) [43], the projector augmented-wave (PAW) potential [44], and the Perdew–Burke–Ernzerhof (PBE) exchange–correlation functional [45]. The 4s and 4p states of Ga, and the 2s and 2p states of O were taken as valence states to reduce the computational cost. The plane-wave basis set was expanded to a cutoff energy of 400 eV to minimize the pulse stress during the structural optimization. The structural optimization was truncated after the Hellmann–Feynman forces were less than 0.01 eV/ \AA . The Brillouin zone was sampled using the gamma-centered method with k -points grid of $1 \times 8 \times 1$. All densities of states were calculated using the hybrid functionals of Heyd, Scuseria, and Ernzerhof

(HSE) [46] with a mixing parameter of 0.32 to fit the experimental bandgaps of $\beta\text{-Ga}_2\text{O}_3$ [47].

Calculation of segregation energy: Because the effect of segregation was modeled as the interstitial site and the substitutional site of point defects, the segregation energy was calculated in two cases. First, the interstitial sites were as follows:

$$E_{\text{seg}(i)} = E_{\text{product}} - E_{\text{reactants}} + n\mu_i \quad (1)$$

where E_p and E_r are the energies of the pristine and segregated abnormal $\beta\text{-Ga}_2\text{O}_3$ homoepitaxial layers, respectively, n is the number of interstitial elements, and μ_i is the chemical potential of the inserted elements. Second, the substitutional sites are as follows:

$$E_{\text{seg}(s)} = E_{\text{product}} - E_{\text{reactants}} - n\mu_{\text{Ga}} + n\mu_s \quad (2)$$

where μ_{Ga} and μ_s are the chemical potentials of Ga and the substituted elements, respectively.

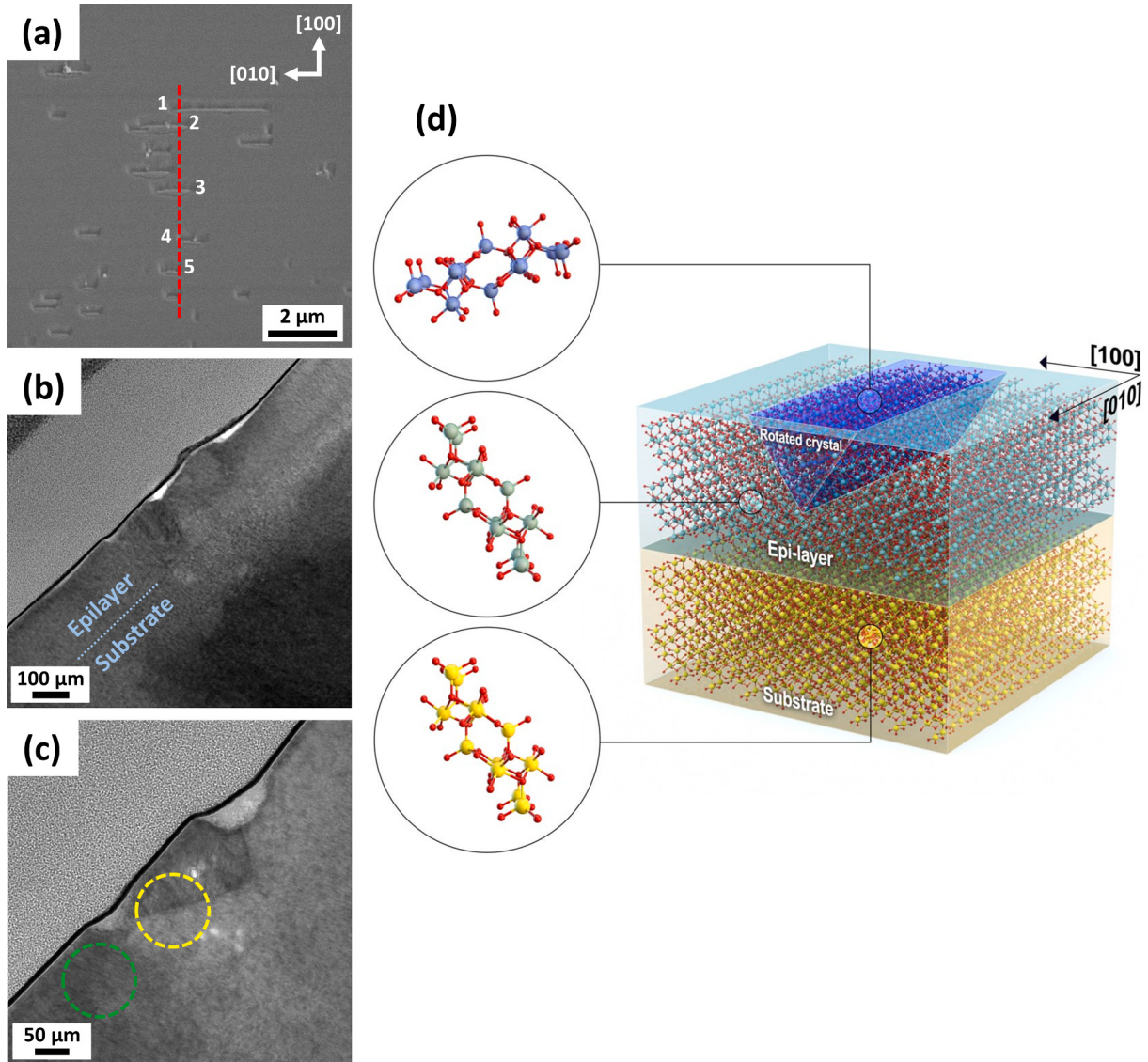


Fig. 1. (a) Scanning electron microscopy (SEM) image showing the rod-like etch pits, where the major axis and minor axis are parallel to the [010] and [100] directions, respectively. Five etch pits were selected for cross-sectional TEM specimen preparation by the FIB method. The TEM specimen was fabricated along the dotted red line, which resulted in the [010] zone axis. (b) At the bottom of the rod-like etch pits a region with different crystallographic orientation compared to the other matrix region was observed. (c) TEM image of one of the etch pits. The shape of the differently orientated region closely resembles a triangle. (d) Illustration of the rotated crystal observed in a (001) $\beta\text{-Ga}_2\text{O}_3$ epilayer, where atomic structures of $\beta\text{-Ga}_2\text{O}_3$ corresponding to the rotated crystal, matrix crystal, and substrate are shown.

3. Results and discussion

First, we performed wet etching of the epilayer sample, and rod-like features appeared on the (001) surface, in which the major axis was parallel to the [010] direction and the minor axis was parallel to the [100] direction of monoclinic β -Ga₂O₃. By forming rod-like etch pits, believed to be formed at the defects, it is easy to recognize the defect positions in Fig. 1(a). A cross-sectional transmission electron microscopy (TEM) specimen was fabricated by the focused ion beam (FIB) method in the region with five rod-like etch pits, and a cross-sectional TEM specimen with the [010] zone axis was prepared. From the low-magnification cross-sectional TEM image, the positions of the five rod-like etch pits were identified (Fig. S1, Supplementary material). Each rod-like etch pit had grooves with a gentle inclination. The grooves corresponded to the outer edge of the major axis of the rod-like pit. At the bottom of the rod-like etch pit in Fig. 1(b), a region showing a different contrast was observed, and the different contrast was caused by a different crystallographic orientation from the matrix epilayer. The shape of the differently orientated region closely resembles a triangle in cross-section view (Fig. 1(c)).

To confirm the different crystallographic orientations at the region under the rod-like etch pit, diffraction patterns were acquired without and with the region under the rod-like etch pit with different orientations (Fig. S2, Supplementary material), and we confirmed the rotated crystal region at the bottom of the rod-like etch pit. Hereafter, we refer to the differently orientated region as “rotated crystal” compared to the “matrix crystal”. The diffraction pattern from the matrix crystal revealed a single-crystalline pattern (Fig. S2a, Supplementary material), while a mixed pattern with an additional single crystalline pattern caused by the rotated crystal was observed in the region with both the matrix and

rotated crystals (Fig. S2b, Supplementary material). Based on the simple diffraction pattern analysis, which will be discussed in Fig. 2 in detail, we concluded that rotated crystals with different crystallographic orientations from the matrix crystal were formed during the homoepitaxial growth of (001) β -Ga₂O₃. Based on the analysed orientation information, Fig. 1(d) illustrates the rotated crystal in the (001) β -Ga₂O₃ epilayer, in which the atomic structures of β -Ga₂O₃ corresponding to the rotated crystal, matrix crystal, and substrate are shown.

The rotated crystals had a specific configuration that was located along the [010] direction with a volumetric portion, as illustrated in Fig. 1(d). In general, the defect density is characterized by the dimensional features of the defects. For example, the dislocation defect density with a one-dimensional line feature is defined as the sum of the total length of dislocations per unit volume of the sample, which results in units of cm^{-2} . In the case of a stacking-fault defect with a two-dimensional plane feature, its density is defined as the sum of the total area of stacking faults per unit volume of the sample, which results in units of cm^{-1} . The rotated crystal illustrated in Fig. 1(d) based on TEM observations has a three-dimensional volumetric feature; therefore, its density can be defined by the sum of the total volume of rotated crystals per unit volume of the sample, which results in a dimensionless unit, which corresponds to the volume ratio. We estimated the volumetric ratio of the rotated crystal to the matrix crystal (see Note 1 and Fig. S3, Supplementary material), which was estimated to be less than 0.0028. This implies that the volumetric portion of the rotated crystals was only 0.28% (maximum) of the total epilayer, which was too small to be easily detected.

Fig. 2(a) shows a high-resolution TEM (HRTEM) image of the rotated crystal and matrix regions. Fig. 2(b) and (c) show diffraction patterns obtained from the rotated and matrix regions, respectively, by fast

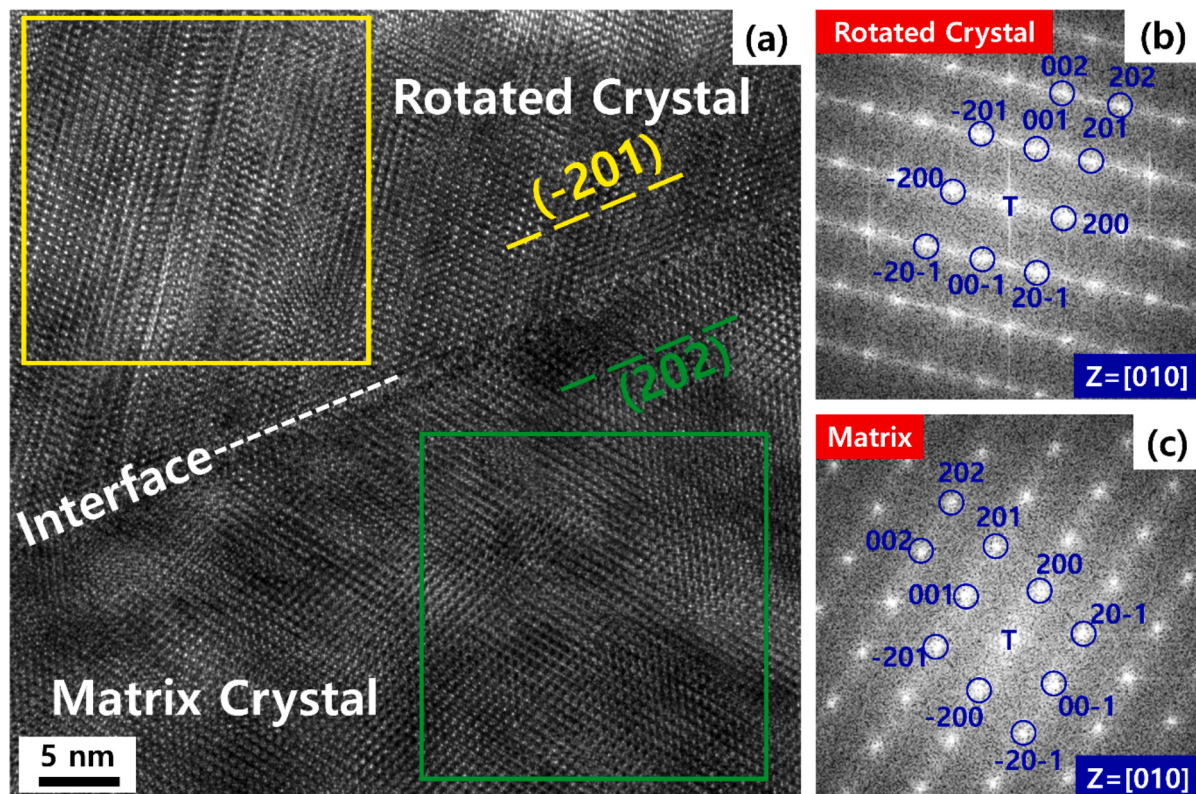


Fig. 2. (a) HRTEM image showing the rotated and matrix crystals forming an interface. At the interface the rotated crystal is the $(\bar{2}01)$ plane and the matrix crystal is the (202) plane. (b) Diffraction pattern obtained by FFT of the region marked by the yellow square in the rotated crystal shown in (a). (c) Diffraction pattern obtained by FFT of the region marked by the green square in the matrix crystal shown in (a). The $(\bar{2}01)$ plane in the rotated crystal is parallel to the (202) plane of the matrix crystal, forming the $(201)/(202)$ interface. The zone axis for both diffraction pattern is $[010]$ and the rotated crystal is rotated counterclockwise with the $[010]$ direction by $\sim 72.5^\circ$.

Fourier transformation (FFT) of the HRTEM images from the marked areas in the image. The zone axes in Fig. 2(b) and (c) are [010] of the monoclinic β -Ga₂O₃. The crystal was rotated $\sim 73^\circ$ relative to the matrix crystal counterclockwise with the [010] axis. This results in the $(\bar{2}01)$ plane of the rotated crystal parallel to the (202) plane of the matrix crystal, and these $(\bar{2}01)$ and (202) planes form an interface between the rotated and matrix crystals. Note that the calculated angle between the $(\bar{2}01)$ and (202) planes of β -Ga₂O₃ was 72.5° , which agrees well with the observed rotation angle (Fig. S4, Supplementary material).

Fig. 3(a) and (b) show the annular bright-field (ABF) and HAADF high-resolution (HR) STEM images acquired at the interface region with the rotated and the matrix crystals. Both gallium (Ga) and oxygen (O) atoms are visible in the ABF-HRSTEM image because it is sensitive to both heavy and light elements, while the bright spots in HAADF-HRSTEM image correspond to the heavy Ga atoms because it shows the atomic number sensitive contrast (so called Z-contrast) nature. These two HRSTEM images clearly revealed the atomic structure at the interface between the rotated and matrix crystals; the interface did not show any amorphous or disordered structures, while periodical structures along the interface were observed in both HRSTEM images. In ABF-HRSTEM and HAADF-HRSTEM images, corresponding atomic structural units were overlaid on the dark and bright spots, respectively. The

$(\bar{2}01)$ plane of the upper crystal (rotated crystal) is facing the (202) plane of the lower crystal (matrix crystal). The Ga atoms indicated by the red circles in Fig. 3(a) and (c) are shared by the facing two crystals and the distance between the shared two Ga atoms is approximately 14.71 Å and 14.73 Å when measured from the upper rotated crystal and lower matrix crystal, respectively. The mismatch between the upper and lower crystals was calculated as follows: $f = (14.73 - 14.71)/14.71 = 0.00136$, which is very close to zero. The mismatch of 0.00136 is almost 100 times smaller than that of (0001) GaN/sapphire interface, which is very popular material system in current blue light emitting diodes. Therefore, the observed $(\bar{2}01)/(202)$ interface was favorably formed by rotating the crystal in the (001) homoepitaxy of β -Ga₂O₃. The atomic positions of the heavy Ga atoms observed in both images are consistent with those at the interface constructed using the stable structure of β -Ga₂O₃, except the deviated Ga atoms indicated by the red arrow in the HAADF-HRSTEM image in Fig. 3(b).

Another interesting atomic structural feature is that the structures had an elongated elliptical shape in the ABF-HRSTEM image, in which the atomic positions of the light O atoms could be observed. The Ga atoms in tetrahedral sites formed a short elliptical shape with the O atoms because the distance between the Ga atoms and the two overlapping O atoms is short when the monoclinic structure of β -Ga₂O₃ is

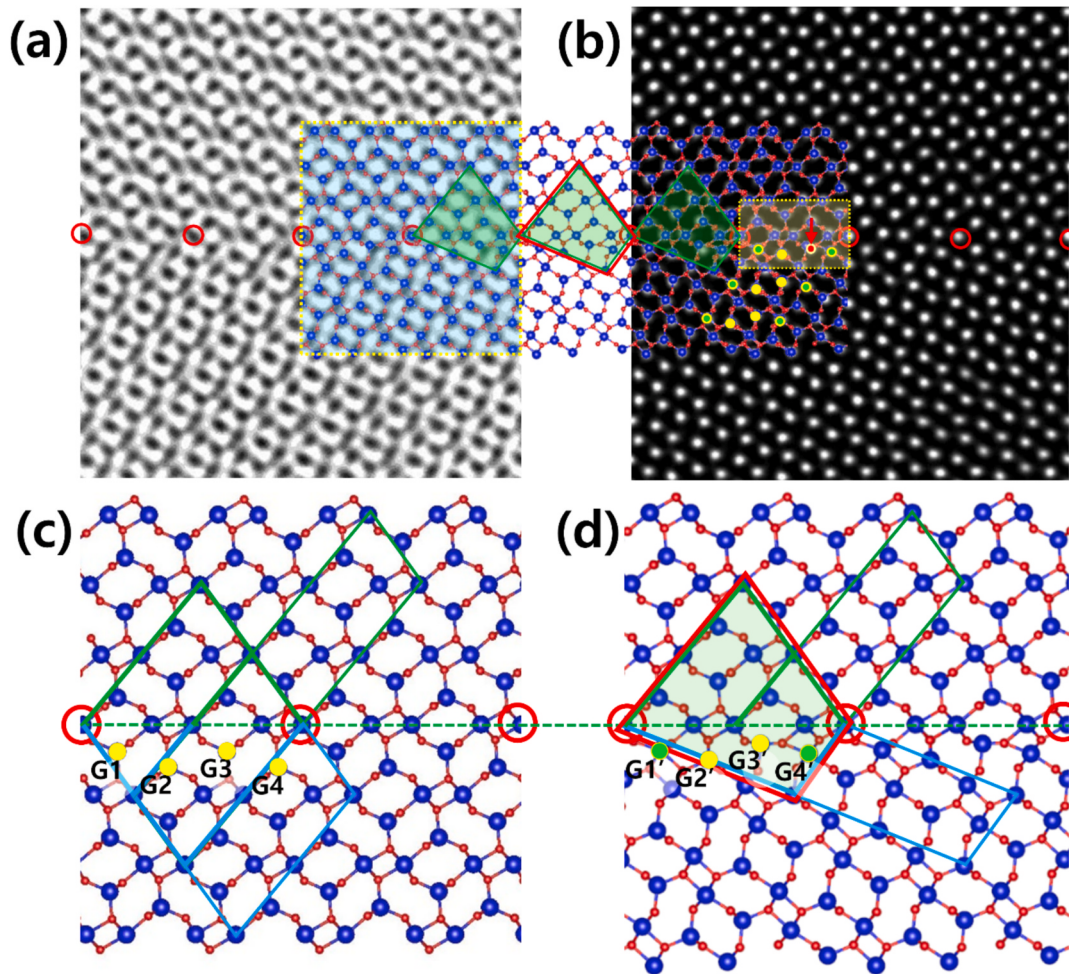


Fig. 3. (a) ABF-HRSTEM image acquired from the rotated crystal and the matrix crystal. (b) HAADF-HRSTEM image acquired from the rotated crystal and the matrix crystal. These two HRSTEM images clearly revealed the atomic structure at the interface between the rotated and matrix crystals; the interface did not show any amorphous or disordered structures, while periodical structures along the interface were observed in both HRSTEM images. The red arrow in (b) indicates the observed Ga atoms deviated from the reference structure. (c) β -Ga₂O₃ structure constructed with only the upper rotated crystal. (d) β -Ga₂O₃ structure constructed by placing the upper rotated crystal and lower matrix crystal facing to each other based on the observed rotational relationship. The Ga atoms indicated by the red circles in (a) and (c) are shared by the facing two crystals. The repeated structure was mentioned by trapezoid at the interface in (d). G1', G2', G3', and G4' in (c) and (d) indicate zigzag Ga atoms below the interface, which belong to octahedral, tetrahedral, and octahedral sites, sequentially.

projected along the [010] direction. The Ga–O pairs in octahedrally coordinated structures appear as long elliptical shapes because the Ga atoms are close to two atomic columns located in two opposite directions when the unit cell is projected along the [010] direction. Fig. 3(c) shows a β -Ga₂O₃ structure constructed using only the upper rotated crystal. Because the crystal has a normal β -Ga₂O₃ structure, the $(\bar{2}01)$ planes are composed of an octahedral Ga atom layer and a tetrahedral site Ga atom layer repeated in a layer-by-layer structure (Fig. S4, Supplementary material). Looking at the structure in more detail, Ga atoms with octahedral sites are located side by side without displacement along the normal direction on the layer (we henceforth, call these Ga atoms “flat” Ga atoms). However, Ga atoms with tetrahedral sites are located side by side with displacement along the normal direction on the layer (we call this Ga atoms as “zigzag” Ga atoms). In the HRSTEM images, because the upper rotated crystal was terminated by the flat Ga atoms in the octahedral sites at the interface, the first Ga atomic layer below the interface has to be located in the zigzag Ga atoms in the tetrahedral sites, as indicated by G1, G2, G3, and G4 in Fig. 3(c). Fig. 3(d) shows β -Ga₂O₃ structure constructed by placing the upper rotated crystal and lower matrix crystal facing to each other based on the observed rotational relationship. That is, the interface plane is the $(\bar{2}01)$ plane belonging to the rotated crystal and it is simultaneously the (202) plane belonging to the matrix crystal. In this case, the first Ga atom layer below the interface formed zigzag Ga atoms, but each Ga atom had to be in the octahedral, tetrahedral, tetrahedral, and octahedral sites, as indicated by G1', G2', G3', and G4' in Fig. 3(d).

Regardless of the difference in the atomic structures between the $(\bar{2}01)$ and (202) planes, the Ga atomic positions on the (202) plane coincide with the zigzag Ga atomic columns on the $(\bar{2}01)$ plane with a slight difference; specifically, the Ga atom at the G1' position of the (202) plane is located at the same position as the Ga atom on the G1 position of the $(\bar{2}01)$ plane. The distinctive difference between the observed HAADF-HRSTEM image and the atomic structure of the (202) plane was found at the Ga atom at position G3', while the other Ga atoms conserved the normal atomic positions on the plane. For a more detailed comparison, we show a magnified image of the interfacial boundary region, which is indicated by the yellow rectangle in the HAADF-HRSTEM image in Fig. 3(b) (inverted contrast used for good

visibility). The determined displacement between the G3' and Ga atoms in the observed STEM image was $\sim 1.03 \text{ \AA}$ as shown in Fig. 4. We assumed that this displacement may be a result of G3 and G3' being paired with different O atoms at the interface boundary as shown in Fig. 4; thereby, a distinctive difference between the observed HAADF-HRSTEM image and the atomic structure of the (202) plane was observed. As a result, the growth of completely different crystalline orientations can be caused by only a slight misalignment-induced atomic displacement.

In order to evaluate the strain state at the interface between the rotated and the matrix crystals, strain analysis was conducted by applying geometric phase analysis (GPA) of the HAADF HR-STEM image (Fig. S5, Supplementary material). From GPA analysis, the strain fields are uniformly and smoothly distributed throughout the rotated crystal, from the edge far from the interface to the interface, indicating that the atomic arrangement is well-conserved. Additionally, when the lattice planes of the matrix crystal are used for GPA, the strains are also uniformly distributed in the crystals. This indicates that the atoms of the rotated and matrix crystals are free from any strain effect owing to the small lattice mismatch.

The grain boundary energy indicates the stability of the mismatched interface. Therefore, based on the energies obtained from the DFT calculations, the grain boundary energy for 16 interfaces was calculated as follows:

$$\sigma_{GB} = \frac{E_{GB} - E_{bulk}}{2A} \quad (3)$$

where E_{GB} and E_{bulk} are the energies of the grain boundary and bulk supercell, respectively, and A is the area of the interface. For the 16 interfaces with different atom configurations interface formation energies were calculated. As shown in Fig. 5(c), surprisingly, their grain boundary energies were very low compared to other oxides in which mismatched interfaces were well formed, such as ZnO [48] and perovskite oxides [49]. This implies that abnormal interfaces are commonly formed in such films. Among the calculated interface energies, O-5 and O-8 configurations show two smallest formation values of 0.00471 and $0.00470 \text{ eV}/\text{\AA}^2$, respectively. These two energy values are almost the same but atom configurations are very different. The O-5 configuration has Ga atoms in tetrahedral, tetrahedral, octahedral, and octahedral

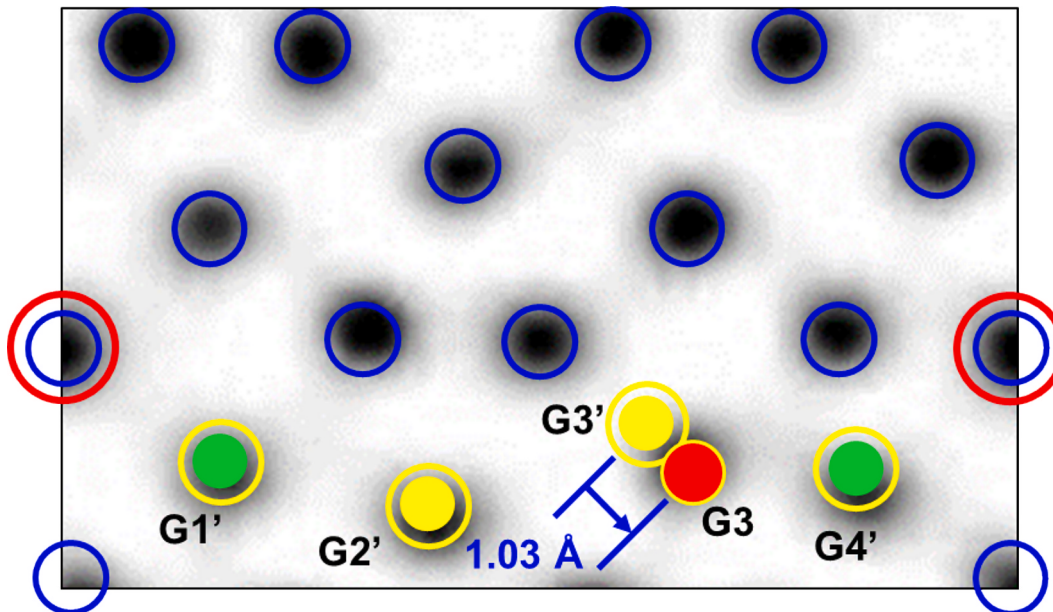


Fig. 4. Magnified ABF-HRSTEM image acquired from the rotated crystal. The yellow and sky-blue lines indicate the Ga atoms placed on tetrahedral and octahedral sites, respectively. The Ga atom just below the interface is located near the octahedral site, not on the row of the tetrahedral sites. The G3' position indicates Ga atom position in the constructed structure but real Ga atom was observed at G3 position marked by red circle, which was deviated by $\sim 1.03 \text{ \AA}$.

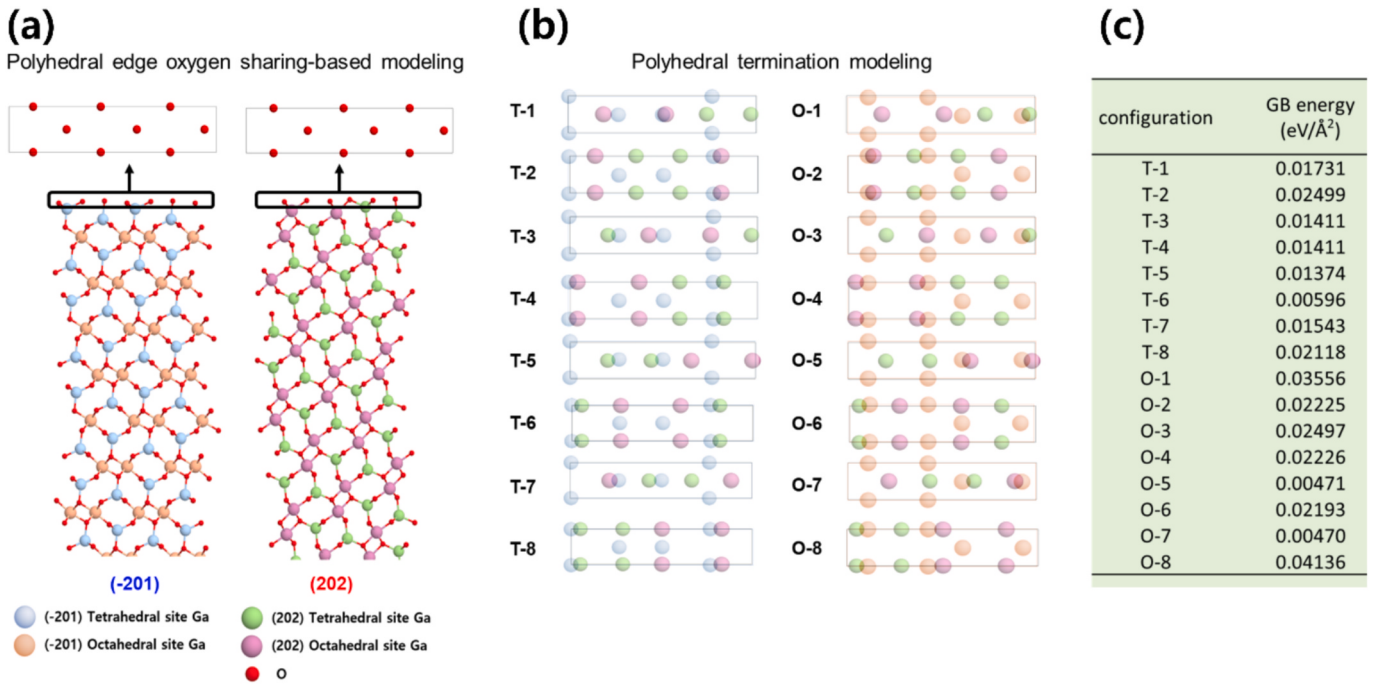


Fig. 5. (a) Schematic of similar oxygen terminations between the (201) and (202) planes. This was confirmed by comparing slabs constructed using the bulk β -Ga₂O₃. (b) Overlapping image of the polyhedral terminations of Ga atoms in both planes. A total of 16 cases were configured. For the (201) planes, two terminations in which only octahedral site or tetrahedral site exist were selected, and eight cases in which octahedral site and tetrahedral sites coexist were selected for the (202) plane. (c) Calculated grain boundary energies of the atomistic models of the abnormal homoepitaxial layer with the 16 cases.

sites in order. However, the O-7 configuration has Ga atoms in octahedral, tetrahedral, tetrahedral, and octahedral sites in order. Here, it should be noted that observed Ga atom configuration was in the octahedral, tetrahedral, tetrahedral, and octahedral sites, as indicated by G1', G2', G3', and G4' in Fig. 3(c) and Fig. 4. Therefore, we can conclude that the interface formation is 0.00470 eV/Å². The calculated interface energy of 0.00470 eV/Å² (=75.3 mJ/m²) is very small in the range of Shockley-type stacking fault energy of GaN.

To understand the electrical properties of the mismatched interface, we calculated the electronic structure of the abnormal homoepitaxial layer. Fig. 6(a) shows the total density of states (TDOS) of bulk β -Ga₂O₃ and the abnormal homoepitaxial layer formed by the rotated crystals. The electronic structure of the abnormal homoepitaxial layer was different from that of the bulk, which implies a change in the electrical properties. Fig. 6(b) shows the magnified TDOS within the energy ranges around the valence band maximum (VBM) and conduction band minimum (CBM) in Fig. 6(a). In the abnormal homoepitaxial layer, shallow and deep defect states are observed around the VBM and the CBM of bulk β -Ga₂O₃, respectively. In particular, the deep states introduced by mismatched interfaces can act as recombination centers, which degrade the electrical properties of β -Ga₂O₃ [11]. Fig. 6(c) shows that the charge of the defects was located at the (201)/(202) interface boundaries by identifying the partial charge density at both states. As shown in Fig. 3, there are no dangling bonds at the (201)/(202) interface. The partial charge density at the (201)/(202) interface are delocalized at polyhedral pairs with octahedrons and tetrahedrons as shown in Fig. 6(c), where the interface position was mentioned by arrows. In case of the VBM, the shallow state is located mostly at the two-octahedron pair as marked by a dotted circle. However, the deep state is located at the octahedron-tetrahedron pair in case of the CBM as marked by a dotted circle. Therefore, we concluded that defect states do not originate from any dangling bonds, but the states are delocalized to different polyhedral pairs. This is because they are differently connected by a slight atomic distortion at the growth interface. Furthermore, we identified that the abnormal homoepitaxial layer had a lower band gap

(approximately 0.9 eV) than the bulk. The formation of an abnormal interface during the growth of a thin film may affect the performance of Ga₂O₃-based electronic devices.

We also investigated whether the segregation of impurities (hydrogen, silicon, or aluminum) can passivate the deep states of the abnormal interface. Hydrogen, which could permeate during growth [50], was inserted into the interstitial site due to its small radius. Silicon, which is widely used as an N-type dopant [51], was substituted for the tetrahedral site owing to its structural nature. Aluminum, which is commonly used to increase the bandgap [52], was substituted on the octahedral site due to its structural stability [47].

Fig. 7(a) shows the pristine, interstitial, and substitutional configurations of the interface boundaries. The possibility of segregation at the interface boundaries was investigated by calculating the formation energies, as listed in Table 1. It was found that segregation on the interface boundaries was more favourable. This means that the segregation effect can preferentially occur at the interface boundary. Fig. 7(b) shows the TDOS of the segregated abnormal homoepitaxial layers compared to the pristine state with bulk β -Ga₂O₃. Silicon and hydrogen create an additional deep state around 3.5 eV. Although the addition of aluminium slightly recovered the decreased band gap, this effect was not sufficient to restore the original bulk band level. Once the rotated crystal on the matrix crystal is formed, it creates deep states, which are difficult to passivate by dopant segregation. Because this degradation is not easily corrected, a strategy to suppress the formation of an abnormal homoepitaxial layer is essential in the future.

4. Conclusions

We found formation of nanoscale rotation crystals in monoclinic β -Ga₂O₃ epitaxy, which formed the (201)/(202) interface boundaries between the rotated crystal and the matrix epilayer. The (201)/(202) planes can be matched without any dangling bonds, even though β -Ga₂O₃ has a low-symmetry monoclinic structure. The volumetric portion of the nanoscale rotated crystals was only 0.28 % (maximum) of

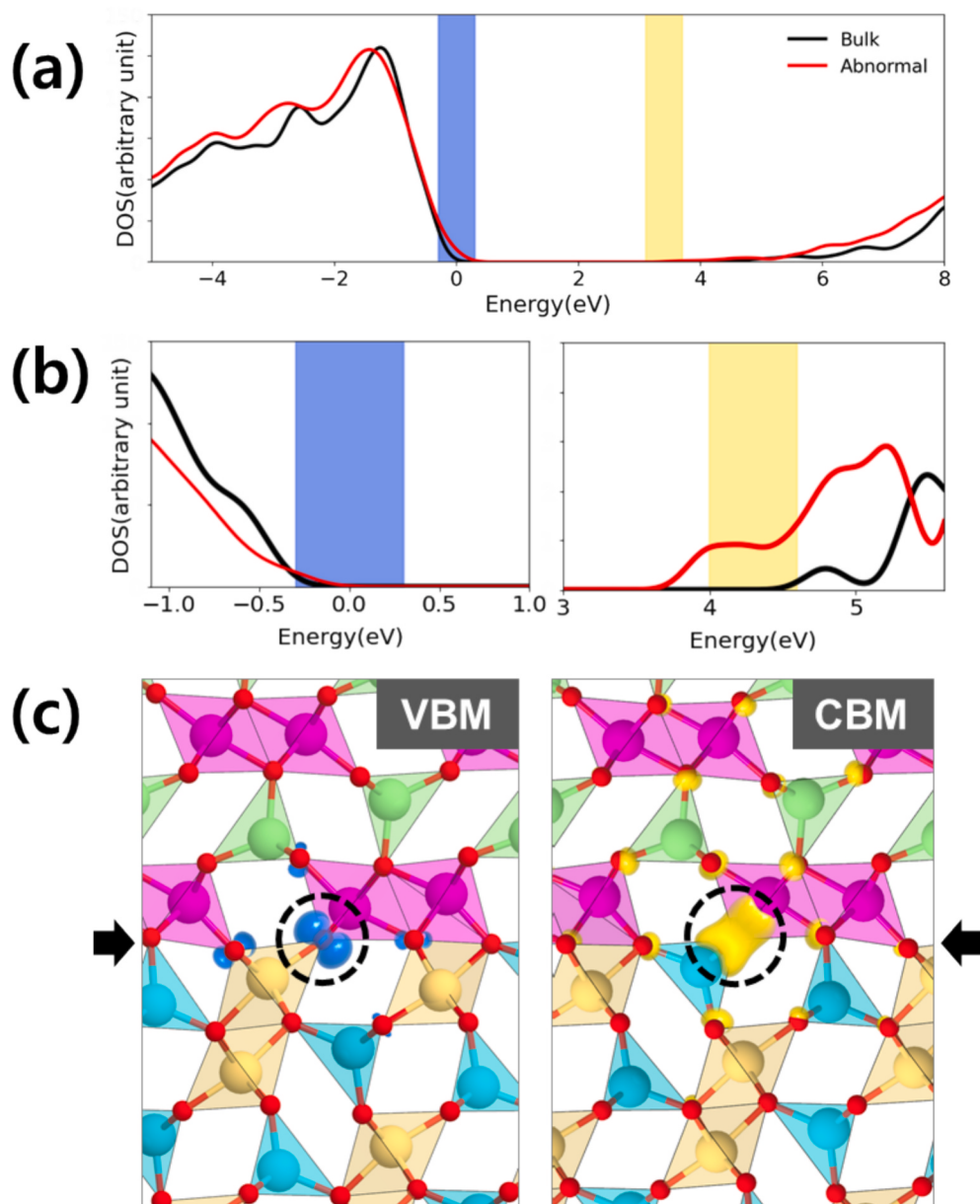


Fig. 6. (a) Calculated TDOS of bulk and the abnormal homoepitaxial layer of β -Ga₂O₃. The shallow and deep states near the VBM and CBM are shaded with royal blue and yellow, respectively. (b) Magnified TDOS within the energy ranges around the VBM and CBM. (c) Charge density of VBM and CBM for the abnormal homoepitaxial layer. Charges in the VBM were mainly observed at the edge shared by octahedrons of the (201) and the (202) faces. In contrast, the charges in CBM were identified at the edge shared by octahedron and tetrahedron of the (201) and the (202) faces as marked by dotted circles. The arrows indicate the position of the interface.

the total epilayer, which was too small to be easily detected. The mismatch at the interface was calculated to be 0.00136, which is very close to zero. From the ADF- and HAADF-HRSTEM investigations, it was found that specific Ga atom displaced $\sim 1.03 \text{ \AA}$, repeatedly and regularly at the interface. Such a sub-nanometer scale displacement was confirmed by comparing the atomic-resolution HAADF-HRSTEM micrography and constructed interface structure. From DFT calculation by using the interface structure constructed based on the ADF- and HAADF-HRSTEM investigation, the interface formation energy was determined to the very small value of $0.00470 \text{ eV}/\text{\AA}^2 (=75.3 \text{ mJ/m}^2)$. In the homoepitaxial layer with the rotated crystals, shallow and deep defect states are observed around the VBM and the CBM of bulk β -Ga₂O₃, respectively. In particular, the deep states introduced by mismatched interfaces can act as recombination centres, which degrade the electrical properties of β -Ga₂O₃. Furthermore, we identified that the interface

results in a lower band gap (approximately 0.9 eV) than the bulk without the interface, which can hinder the achievement of theoretical device performance. Moreover, once degraded, it is difficult to restore the original bulk band level, even via dopant segregation of H, Si, and Al, which are known to significantly affect the electronic structure. The segregation of impurities (hydrogen, silicon, or aluminium) on the interface boundaries was more favourable. However, the decreased band gap was not restored by the impurity segregations. Our findings provide a fundamental understanding into the atomic-scale interfacial structure at the locally formed nanoscale defect and their electronic property.

CRediT authorship contribution statement

Trong Si Ngo: Writing – original draft, Investigation, Data curation.

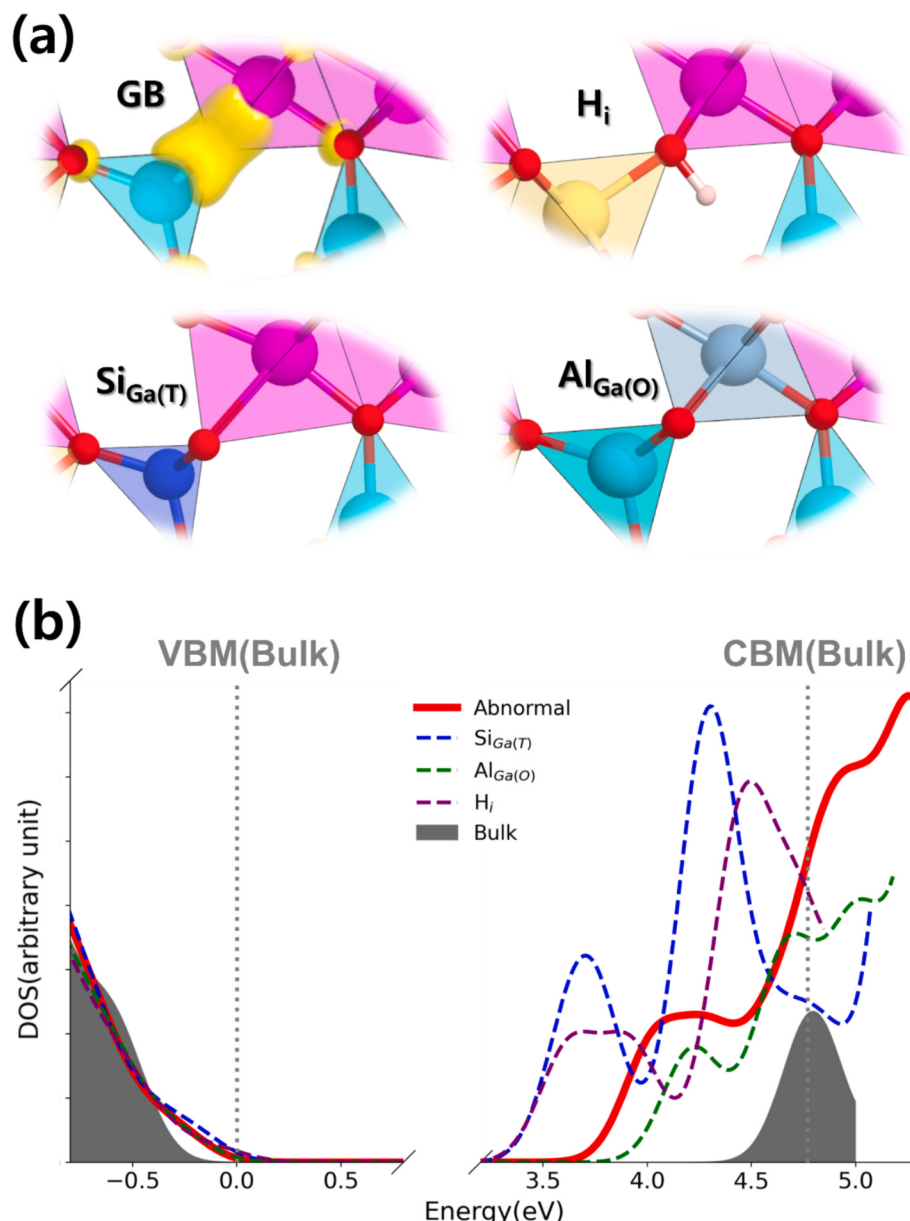


Fig. 7. Investigation of the effect of segregation on the abnormal homoepitaxial layer. The segregation is simulated as point defects. (a) Configurations of pristine, interstitial, and substitutional sites at the interface boundary where deep level state occurs. H is inserted into interface boundary region. Si and Al are substituted for the tetrahedral (T) and octahedral (O) sites, respectively. (b) Comparison of TDOS among pristine and segregated abnormal homoepitaxial layers with bulk β -Ga₂O₃.

Table 1
Calculated segregation energies of the abnormal homoepitaxial layer segregated into non-interface area and interface boundary.

Segregation energy (eV)		
Segregated atom	Segregated location	
	Non-interface area	Interface boundary
Si	-1.56	-1.84
Al	-3.32	-3.37
H	2.60	-1.19

Soon-Ku Hong: Writing – review & editing, Writing – original draft, Supervision, Resources, Methodology, Investigation, Formal analysis, Data curation, Conceptualization. **Hyeon Woo Kim:** Software, Methodology, Data curation. **Sung Beom Cho:** Visualization, Validation, Software, Methodology, Data curation. **Young Heon Kim:** Validation,

Software, Investigation, Formal analysis, Data curation. **Nguyen Quoc Vuong:** Validation, Data curation. **Hu Young Jeong:** Investigation, Data curation. **Raouf Hayyak:** Visualization, Data curation. **Taswar Iqbal:** Visualization, Data curation. **Dae-Woo Jeon:** Investigation, Data curation. **Ji-Hyeon Park:** Visualization, Data curation. **Jae Kyoung Mun:** Validation, Data curation.

Declaration of competing interest

The authors declare that they have no known competing financial interests or personal relationships that could have appeared to influence the work reported in this paper.

Acknowledgements

This research was supported by National Research Foundation of Korea (NRF) (grant No. (2020R1I1A3073787, 2020M3H4A3081797,

and 2024M3H4A3A01046532).

Appendix A. Supplementary material

Supplementary data to this article can be found online at <https://doi.org/10.1016/j.apsusc.2025.163471>.

Data availability

Data will be made available on request.

References

- [1] J.K. Mun, K. Cho, W. Chang, H.-W. Jung, J. Do, Editors' choice—2.32 kv breakdown voltage lateral β -Ga₂O₃ MOSFETs with source-connected field plate, *ECS J. Solid State Sci. Technol.* 8 (2019) Q3079–Q3082, <https://doi.org/10.1149/2.0151907jss>.
- [2] Z. Xia, C. Joishi, S. Krishnamoorthy, S. Bajaj, Y. Zhang, M. Brenner, S. Lodha, S. Rajan, Delta doped β -Ga₂O₃ field effect transistors with regrown Ohmic contacts, *IEEE Electron. Device Lett.* 39 (2018) 568–571, <https://doi.org/10.1109/LED.2018.2805785>.
- [3] D. Zhang, W. Zheng, R.C. Lin, T.T. Li, Z.J. Zhang, F. Huang, High quality β -Ga₂O₃ film grown with N₂O for high sensitivity solar-blind-ultraviolet photodetector with fast response speed, *J. Alloys Compd.* 735 (2018) 150–154, <https://doi.org/10.1016/j.jallcom.2017.11.037>.
- [4] J.H. Kang, L. Xie, Y. Wang, H. Lee, N. Campbell, J. Jiang, P.J. Ryan, D.J. Keavney, J.W. Lee, T.H. Kim, X. Pan, L.Q. Chen, E.E. Hellstrom, M.S. Rzchowski, Z.K. Liu, C. B. Eom, Control of epitaxial BaFe₂As₂ atomic configurations with substrate surface terminations, *Nano Lett.* 18 (2018) 6347–6352, <https://doi.org/10.1021/acs.nanolett.8b02704>.
- [5] T.S. Ngo, D.D. Le, J. Lee, S.K. Hong, J.S. Ha, W.S. Lee, Y.B. Moon, Investigation of defect structure in homoepitaxial (201) β -Ga₂O₃ layers prepared by plasma-assisted molecular beam epitaxy, *J. Alloys. Compd.* 834 (2020) 155027, <https://doi.org/10.1016/j.jallcom.2020.155027>.
- [6] S. Sasano, R. Ishikawa, G. Sánchez-Santolino, H. Ohta, N. Shibata, Y. Ikuhara, Atomistic origin of Li-Ion conductivity reduction at (Li₃La_{2/3}x)TiO₃ grain boundary, *Nano Lett.* 21 (2021) 6282–6288, <https://doi.org/10.1021/acs.nanolett.1c02174>.
- [7] J. Wei, T. Ogawa, B. Feng, T. Yokoi, R. Ishikawa, A. Kuwabara, K. Matsunaga, N. Shibata, Y. Ikuhara, Direct measurement of electronic band structures at oxide grain boundaries, *Nano Lett.* 20 (2020) 2530–2536, <https://doi.org/10.1021/acs.nanolett.9b05298>.
- [8] G. Schusteritsch, T. Ogawa, B. Feng, T. Yokoi, R. Ishikawa, A. Kuwabara, K. Matsunaga, N. Shibata, Y. Ikuhara, Direct measurement of electronic band structures at oxide grain boundaries, *Nano Lett.* 20 (2020) 2530–2536, <https://doi.org/10.1021/acs.nanolett.9b05298>.
- [9] J.M. Johnson, Z. Chen, J.B. Varley, C.M. Jackson, E. Farzana, Z. Zhang, A. R. Arehart, H.L. Huang, A. Genc, S.A. Ringel, C.G. Van De Walle, D.A. Muller, J. Hwang, Unusual formation of point-defect complexes in the ultrawide-band-gap semiconductor β -Ga₂O₃, *Phys. Rev.X* 9 (2019) 041027, <https://doi.org/10.1103/PhysRevX.9.041027>.
- [10] J. Wei, B. Feng, R. Ishikawa, T. Yokoi, K. Matsunaga, N. Shibata, Y. Ikuhara, Direct imaging of atomistic grain boundary migration, *Nat. Mater.* 20 (2021) 951–955, <https://doi.org/10.1038/s41563-020-00879-z>.
- [11] A.Y. Polyakov, N.B. Smirnov, I.V. Shchemerov, E.B. Yakimov, J. Yang, F. Ren, G. Yang, J. Kim, A. Kuramata, S.J. Pearton, Point defect induced degradation of electrical properties of Ga₂O₃ by 10 MeV proton damage, *Appl. Phys. Lett.* 112 (2018) 032107, <https://doi.org/10.1063/1.5012993>.
- [12] S.J. Pearton, J. Yang, P.H. Cary, F. Ren, J. Kim, M.J. Tadjer, M.A. Mastro, A review of Ga₂O₃ materials, processing, and devices, *Appl. Phys. Rev.* 5 (2018) 011301, <https://doi.org/10.1063/1.5006941>.
- [13] M.A. Mastro, A. Kuramata, J. Calkins, J. Kim, F. Ren, S.J. Pearton, Perspective—opportunities and future directions for Ga₂O₃, *ECS J. Solid State Sci. Technol.* 6 (2017) P356–P359, <https://doi.org/10.1149/2.0031707jss>.
- [14] K. Sasaki, M. Higashiwaki, A. Kuramata, T. Masui, S. Yamakoshi, Ga₂O₃ schottky barrier diodes fabricated by using single-crystal β -Ga₂O₃ (010) substrates, *IEEE Electron. Device Lett.* 34 (2013) 493–495, <https://doi.org/10.1109/LED.2013.2244057>.
- [15] M. Higashiwaki, K. Konishi, K. Sasaki, K. Goto, K. Nomura, Q.T. Thieu, R. Togashi, H. Murakami, Y. Kumagai, B. Monemar, A. Koukitu, A. Kuramata, S. Yamakoshi, Temperature-dependent capacitance–voltage and current–voltage characteristics of Pt/Ga₂O₃ diodes fabricated on n[–]Ga₂O₃ (001) Schottky barrier drift layers grown by halide vapor phase epitaxy, *Appl. Phys. Lett.* 108 (2016) 133503, <https://doi.org/10.1063/1.4945267>.
- [16] K. Konishi, K. Goto, H. Murakami, Y. Kumagai, A. Kuramata, S. Yamakoshi, M. Higashiwaki, 1-kV vertical Ga₂O₃ field-plated Schottky barrier diodes, *Appl. Phys. Lett.* 110 (2017) 103506, <https://doi.org/10.1063/1.4977857>.
- [17] K. Sasaki, D. Wakimoto, Q.T. Thieu, Y. Koishikawa, A. Kuramata, M. Higashiwaki, S. Yamakoshi, First demonstration of Ga₂O₃ trench MOS-type schottky barrier diodes, *IEEE Electron. Device Lett.* 38 (2017) 783–785, <https://doi.org/10.1109/LED.2017.2696986>.
- [18] J. Yang, S. Ahn, F. Ren, S.J. Pearton, S. Jang, A. Kuramata, High breakdown voltage (-201) β -Ga₂O₃ schottky rectifiers, *IEEE Electron. Device Lett.* 38 (2017) 906–909, <https://doi.org/10.1109/LED.2017.2703609>.
- [19] T. Watahiki, Y. Yuda, A. Furukawa, M. Yamamuka, Y. Takiguchi, S. Miyajima, Heterojunction p-Cu₂O/n-Ga₂O₃ diode with high breakdown voltage, *Appl. Phys. Lett.* 111 (2017) 222104, <https://doi.org/10.1063/1.4998311>.
- [20] M. Higashiwaki, Y. Yuda, A. Furukawa, M. Yamamuka, Y. Takiguchi, S. Miyajima, Heterojunction p-Cu₂O/n-Ga₂O₃ diode with high breakdown voltage, *Appl. Phys. Lett.* 111 (2017) 222104, <https://doi.org/10.1063/1.4998311>.
- [21] M. Higashiwaki, K. Sasaki, T. Kamimura, M. Hoi Wong, D. Krishnamurthy, A. Kuramata, T. Masui, S. Yamakoshi, Depletion-mode Ga₂O₃ metal-oxide-semiconductor field-effect transistors on β -Ga₂O₃ (010) substrates and temperature dependence of their device characteristics, *Appl. Phys. Lett.* 103 (2013) 123511, <https://doi.org/10.1063/1.4821858>.
- [22] M.H. Wong, K. Sasaki, A. Kuramata, S. Yamakoshi, M. Higashiwaki, Field-plated Ga₂O₃ MOSFETs with a breakdown voltage of over 750 V, *IEEE Electron. Device Lett.* 37 (2016) 212–215, <https://doi.org/10.1109/LED.2015.2512279>.
- [23] A.J. Green, K.D. Chabak, E.R. Heller, R.C. Fitch, M. Baldini, A. Fiedler, K. Irmscher, G. Wagner, Z. Galazka, S.E. Tetlak, A. Crespo, K. Leedy, G.H. Jessen, 3.8-MV/cm breakdown strength of MOVPE-grown Sn-Doped β -Ga₂O₃ MOSFETs, *IEEE Electron. Device Lett.* 37 (2016) 902–905, <https://doi.org/10.1109/LED.2016.2568139>.
- [24] Z. Hu, K. Nomoto, W. Li, N. Tanen, K. Sasaki, A. Kuramata, T. Nakamura, D. Jena, H.G. Xing, Enhancement-mode Ga₂O₃ vertical transistors with breakdown voltage >1kV, *IEEE Electron. Device Lett.* 39 (2018) 869–872, <https://doi.org/10.1109/LED.2018.2830184>.
- [25] K. Zeng, A. Vaidya, U. Singisetti, 1.85 kV breakdown voltage in lateral field-plated Ga₂O₃ MOSFETs, *IEEE Electron. Device Lett.* 39 (2018) 1385–1388, <https://doi.org/10.1109/LED.2018.2859049>.
- [26] J. Zhang, J. Shi, D.C. Qi, L. Chen, K.H.L. Zhang, Recent progress on the electronic structure, defect, and doping properties of Ga₂O₃, *APL Mater.* 8 (2020) 020906, <https://doi.org/10.1063/1.5142999>.
- [27] G. Wagner, M. Baldini, D. Gogova, M. Schmidbauer, R. Schewski, M. Albrecht, Z. Galazka, D. Klimm, R. Fornari, Homoepitaxial growth of β -Ga₂O₃ layers by metal-organic vapor phase epitaxy, *Phys. Status Solidi A* 211 (2014) 27–33, <https://doi.org/10.1002/pssa.201330092>.
- [28] E. Ahmadi, E. Ahmadi, Y. Oshima, Materials issues and devices of α - And β -Ga₂O₃, *J. Appl. Phys.* 126 (2019) 160901, <https://doi.org/10.1063/1.5123213>.
- [29] Y. Yao, Y. Sugawara, Y. Ishikawa, Identification of Burgers vectors of dislocations in monoclinic β -Ga₂O₃ via synchrotron x-ray topography, *J. Appl. Phys.* 127 (2020) 205110, <https://doi.org/10.1063/5.0007229>.
- [30] S. Sdoeung, K. Sasaki, K. Kawasaki, J. Hirabayashi, A. Kuramata, T. Oishi, M. Kasu, Origin of reverse leakage current path in edge-defined film-fed growth (001) β -Ga₂O₃ Schottky barrier diodes observed by high-sensitive emission microscopy, *Appl. Phys. Lett.* 117 (2020) 022106, <https://doi.org/10.1063/5.0012794>.
- [31] Y. Yao, Y. Ishikawa, Y. Sugawara, Dislocation classification of a large-area β -Ga₂O₃ single crystal via contrast analysis of affine-transformed X-ray topographs, *J. Cryst. Growth* 548 (2020) 125825, <https://doi.org/10.1016/j.jcrysgro.2020.125825>.
- [32] Y. Yao, K. Hirano, Y. Sugawara, K. Sasaki, A. Kuramata, Y. Ishikawa, Observation of dislocations in thick β -Ga₂O₃ single-crystal substrates using Borrman effect synchrotron x-ray topography, *APL Mater.* 10 (2022) 051101, <https://doi.org/10.1063/5.0088701>.
- [33] Y. Yao, Y. Tsusaka, K. Sasaki, A. Kuramata, Y. Sugawara, Y. Ishikawa, Large-area total-thickness imaging and Burgers vector analysis of dislocations in β -Ga₂O₃ using bright-field x-ray topography based on anomalous transmission, *Appl. Phys. Lett.* 121 (2022) 012105, <https://doi.org/10.1063/5.0098942>.
- [34] M.I. Chaman, K. Hoshikawa, S. Sdoeung, M. Kasu, High crystal quality of vertical Bridgman and edge-defined film-fed growth β -Ga₂O₃ bulk crystals investigated using high-resolution X-ray diffraction and synchrotron X-ray topography, *Jpn. J. Appl. Phys.* 61 (2022) 055501, <https://doi.org/10.35848/1347-4065/ac55e3>.
- [35] Y. Yao, Y. Tsusaka, K. Hirano, K. Sasaki, A. Kuramata, Y. Sugawara, Y. Ishikawa, Three-dimensional distribution and propagation of dislocations in β -Ga₂O₃ revealed by Borrman effect x-ray topography, *J. Appl. Phys.* 134 (2023) 155104, <https://doi.org/10.1063/5.0169526>.
- [36] P. Wang, J. Fan, Y. Lei, T. Hou, Y. Dong, Y. Li, Z. Jia, X. Tao, W. Mu, Bent-shaped twin boundary in β -Ga₂O₃ crystals, *Cryst. Growth Des.* 24 (2024) 7990–7998, <https://doi.org/10.1021/acs.cgd.4c00875>.
- [37] M. Wang, S. Mu, J.S. Speck, C.G. Van de Walle, First-principles study of twin boundaries and stacking faults in β -Ga₂O₃, *Adv. Mater. Interf.* 18 (2023) 23003, <https://doi.org/10.1002/admi.202300318>.
- [38] N.A. Mahadik, M.J. Tadher, P.L. Bonanno, K.D. Hobart, R.E. Stahlbush, T. J. Anderson, A. Kuramata, High-resolution dislocation imaging and microstructural analysis of HVPE- β -Ga₂O₃ films using monochromatic synchrotron topography, *APL Mater.* 7 (2019) 022513, <https://doi.org/10.1063/1.5051633>.
- [39] S. Sdoeung, Y. Otsubo, K. Sasaki, A. Kuramata, M. Kasu, Killer defect responsible for reverse leakage current in halide vapor phase epitaxial (011) β -Ga₂O₃ Schottky barrier diodes investigated via ultrahigh sensitive emission microscopy and synchrotron x-ray topography, *Appl. Phys. Lett.* 123 (2023) 122101, <https://doi.org/10.1063/5.0170398>.
- [40] S. Sdoeung, K. Sasaki, S. Masuya, K. Kawasaki, J. Hirabayashi, A. Kuramata, M. Kasu, Stacking faults: origin of leakage current in halide vapor phase epitaxial (001) β -Ga₂O₃ Schottky barrier diodes, *Appl. Phys. Lett.* 118 (2021) 172106, <https://doi.org/10.1063/5.0049761>.
- [41] K. Ogawa, K. Kobayashi, N. Hasuike, T. Isshiki, Crystal structure analysis of stacking faults through scanning transmission electron microscopy of β -Ga₂O₃ (001) layer grown via halide vapor phase epitaxy, *J. Vac. Sci. Technol. A* 40 (2022) 032701, <https://doi.org/10.1116/6.0001799>.

- [42] L. Meng, D. Yu, H.L. Huang, C. Chae, J. Hwang, H. Zhao, MOCVD growth of β -Ga₂O₃ on (001) Ga₂O₃ substrates, Cryst. Growth Des. 24 (2024) 3737–3745, <https://doi.org/10.1021/acs.cgd.4c00060>.
- [43] G. Kresse, J. Furthmüller, Efficient iterative schemes for ab initio total-energy calculations using a plane-wave basis set, Phys. Rev. B. 54 (1996) 11169–11186, <https://doi.org/10.1103/PhysRevB.54.11169>.
- [44] P.E. Blochl, Projector augmented-wave method, Phys. Rev. B. 50 (1994) 17953–17979, <https://doi.org/10.1103/PhysRevB.50.17953>.
- [45] J.P. Perdew, K. Burke, M. Ernzerhof, generalized gradient approximation made simple, Phys. Rev. Lett. 77 (1996) 3865–3868, <https://doi.org/10.1103/PhysRevLett.77.3865>.
- [46] J. Heyd, G.E. Scuseria, M. Ernzerhof, Hybrid functionals based on a screened Coulomb potential, J. Chem. Phys. 118 (2003) 8207–8215, <https://doi.org/10.1063/1.1564060>.
- [47] H.W. Kim, H. Ko, Y.C. Chung, S.B. Cho, Heterostructural phase diagram of Ga₂O₃-based solid solution with Al₂O₃, J. Eur. Ceram. Soc. 41 (2021) 611–616, <https://doi.org/10.1016/j.jeurceramsoc.2020.08.067>.
- [48] F. Oba, H. Ohta, Y. Sato, H. Hosono, T. Yamamoto, Y. Ikuhara, Atomic structure of [0001]-tilt grain boundaries in ZnO: a high-resolution TEM study of fiber-textured thin films, Phys. Rev. B. 70 (2004) 125415, <https://doi.org/10.1103/PhysRevB.70.125415>.
- [49] J.A. Dawson, I. Tanaka, Local structure and energetics of Pr- and La-doped SrTiO₃ grain boundaries and the influence on core–shell structure formation, J. Phys. Chem. C. 118 (2014) 25765–25778, <https://doi.org/10.1021/jp508444k>.
- [50] K. Goto, K. Ikenaga, N. Tanaka, M. Ishikawa, H. Machida, Y. Kumagai, Thermodynamic and experimental studies of β -Ga₂O₃ growth by metalorganic vapor phase epitaxy, Jpn. J. Appl. Phys. 60 (2021) 045505, <https://doi.org/10.35848/1347-4065/abec9d>.
- [51] J.B. Varley, J.R. Weber, A. Janotti, C.G. Van De Walle, Oxygen vacancies and donor impurities in β -Ga₂O₃, Appl. Phys. Lett. 97 (2010) 142106, <https://doi.org/10.1063/1.3499306>.
- [52] X. Ma, Y. Zhang, L. Dong, R. Jia, First-principles calculations of electronic and optical properties of aluminum-doped β -Ga₂O₃ with intrinsic defects, Res. Phys. 7 (2017) 1582–1589, <https://doi.org/10.1016/j.rinp.2017.04.023>.